

# A Molecular Dynamics Study of Tribological Properties of Silicon Carbide as a Metal-Free Friction Material

Yizhan Zhang, Cortney LeNeave, and Yun-Bo Yi University of Denver

**Citation:** Zhang, Y., LeNeave, C., and Yi, Y.-B., "A Molecular Dynamics Study of Tribological Properties of Silicon Carbide as a Metal-Free Friction Material," SAE Technical Paper 2021-01-1284, 2021, doi:10.4271/2021-01-1284.

## **Abstract**

riction materials containing metal ingredients used in the automotive industry can cause unfavorable environmental impacts. Existing laws and regulations require heavy metals in brake pads to be phased out of production. Substitutions for metals in friction materials, however, may introduce operational safety issue and other unforeseen problems. In the current study, a molecular dynamics model based on LAMMPS has been developed to study the effect of material composition, density, and geometric configurations on the tribological, mechanical, and thermal properties of silicon carbide under various contact conditions at the atomic level. Simulations which incorporate interfacial contact

between surface asperities were performed to predict the elastic modulus, thermal conductivity, wear rate, and coefficient of friction. The resulting predicted properties may help enhance the performance of engineered metal-free friction materials against thermal-mechanical failures. The following factors have been taken into consideration in the model: elevated temperature, sliding speed, crystal orientation, particle size, degree of intersection, types of loading, and surface contact. Some of the simulation results have been compared to existing experimental data found in literature and have proven to be sufficiently accurate. The molecular dynamics model developed in this study can be modified to deal with other types of nonmetallic friction composites.

## 1. Introduction

riction materials are used to generate friction to reduce relative motion by transforming kinetic energy to thermal energy in aircraft, automobiles, and industrial applications among others. Depending on the application, friction materials may consist of phenolic resin, ceramics, advanced fibers, graphitics, metals, and metal alloys. Friction material formulations may include various ingredients to alter a material wear resistance, thermal stability, and mechanical strength  $[\underline{1}, \underline{2}]$ . Typically, automotive brake pads consist of embedded macro- and micro-constituents in cured phenolic resin. For example, most automotive brake pads include macro-particles of copper which reduce localized overheating due to coppers excellent thermal conductivity [3, 4]. Existing laws and regulations in some regions require copper and other heavy metals in brake pads to be phased-out, thereby reducing brake worn copper particulates contamination of stormwater and nearby waterways. Elevated levels of copper are toxic to aquatic life and adversely affect the survival, reproduction, and growth of fish, invertebrates, plants, and amphibians [5]. Graphite, carbon fibers, nanotubes, minerals, and ceramics are potential replacements for metals in friction materials; however, implementation of these materials may introduce operational safety issues. For instance, in brakes, clutches, seals, and bearings a disturbance in the contact pressure can change the rate of frictional heating [6, 7] altering the thermal

stresses and pressure distribution leading to thermal-mechanical instabilities. It is therefore important to investigate metal-free friction materials using multiscale modelling to understand how material properties affect the mechanical responses due to frictional heating and thus the conditions in which the materials fail. Such multiscale investigations are equally important because by substituting metal-contained materials for non-metal materials there may be many new unforeseen issues. It may also be difficult or time-consuming to design an experiment which uses the friction process to determine material properties. With this consideration, a simulation using molecular dynamics (MD) is a logical solution. MD is a relatively new and powerful tool utilizing modern high-performance computers to simulate complex systems at the microscopic level. Using MD simulation, it is faster to achieve a realistic experiment environment and explore a wide array of material properties on a small scale compared to real world experiments. This could quickly provide new insight on investigating novel friction materials or explain the cause of certain phenomenon involving friction in a more fundamental way.

In this paper, the material properties of SiC, a typical material for making brake pads and discs, were evaluated using MD simulation. The intent of the simulation was to find out the frictional, mechanical, and thermal characteristics of the material showing each factor frictional effect on

an atomic scale. This research lays the groundwork for studying the primary cause of thermal-mechanical instabilities (TMI) in sliding friction systems. It may also give information on developing new metal-free friction materials which can prevent or mitigate TMI; a meaningful development across many industries. In this investigation, Large-scale Atomic/Molecular Massively Parallel Simulator (LAMMPS) [8], a classical MD code, was used to characterize the simulations of friction, tensile, and thermal conductivity testing with the assistance of a visualization software Ovito [9]. This research may give some viewpoints on understanding the fundamental mechanism of tribology and provide new possible ways on improving the performance of friction materials at the micro scale.

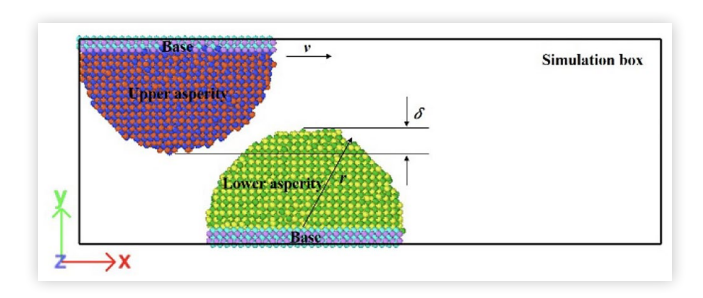
## 2. Methodology of Simulation

### 2.1. Friction Simulation

At the macroscopic level, the dry friction process can be described by Amonton's law:

$$F = \mu N \tag{1}$$

where F is the frictional force,  $\mu$  is the coefficient of friction, and N is the normal force. This law describes material interactions dealing with macrostructures. However, at the microscopic level the situation may be different. Because the scale has been changed to deal with the atomic structure, which examines atoms or molecules, the influence of interatomic bonds and potentials cannot be ignored. The interaction between atoms produces an attraction or repulsion and acts as an additional force during friction. This additional force acts like adhesion where two friction materials attract each other. This kind of contribution is proportional to the number of interatomic bonds that are broken and reformed when the surfaces of two objects slide past each other [10]. The number of interatomic bonds is related to the contact area between the two sliding surfaces. With this extra influence, the normal force can even be negative which means the two friction objects have a very limited contact area or a small gap between them. This is a unique phenomenon which occurs on the atomic scale, it suggests that different results could be found when compared to a macro scale analysis. The MD model for friction simulation focuses on the process on the atomic scale. Basically, there are two kinds of cases that describe the friction process at such a small size [11]. One case uses two asperities as research objects. The main reason is that at the macroscopic level the contact surfaces between friction materials can be treated as ideal flat planes. However, the geometry of the surface is not smooth at an atomistic level. There could always exist some peaks and valleys but in very small sizes such that they are ignored in traditional macroscopic experiments. The other case uses an asperity sliding on a relatively smooth slab. A smooth surface is less common at the nano level, but it is still a possible situation. In this paper, only asperity-asperity friction was considered since it is much FIGURE 1 Schematic of asperity-asperity SiC friction model



more common on an atomistic scale. For asperity-asperity shear, the 3D model was created using upper and lower asperities, and is shown below through Ovito:

Two hemispherical asperities were built in a cuboid simulation box. Si atoms are shown in blue and green, while C atoms are shown in red and yellow. One asperity is at the upper position of the box while the other is at the lower position of the box. Both asperities were connected to bases, which were also made from SiC, and were used for moving or fixing the asperities. First, the lower asperity and lower base were fixed to the initial position as exhibited in Figure 1. Next, a constant velocity was added to the upper base to drive the corresponding upper asperity in the positive x-direction. This gives the upper asperity a relative velocity to the lower asperity. Periodic boundary conditions (PBC) were applied in the x and z directions, while a non-periodic and shrink-wrapped boundary condition was applied in the y direction. During the simulation, constant energy, constant volume (NVE) ensemble was applied to the asperities.

In this work, only 3C-SiC (or  $\beta$ -SiC, zinc blende cubic structure with lattice constant of 4.3596 Å) was considered. The timestep was set to be 0.001 ps. For each timestep, the forces acting on the atoms were calculated from the derivative of the potential, the position, and the velocity and are obtained using velocity-Verlet method [12]. Vashishta potential, which is used to compute the combined 2-body and 3-body family of potentials in inorganic compounds, was implemented for the silicon carbide system in all the simulations mentioned in this paper. This kind of potential is derived from the research made by Priya Vashishta et al. [13]. The basic formula for the total potential energy of the system is given by:

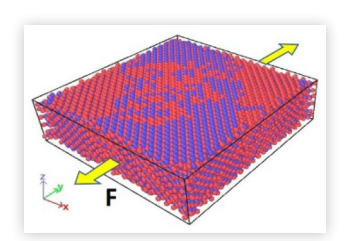
$$E = \sum_{i < j} E_{ij}^{(2)} (r_{ij}) + \sum_{i,j < k} E_{ijk}^{(3)} (r_{ij}, r_{jk})$$
 (2)

Where in this expression, the first and second term represent the two-body part and three-body part of the effective potential, respectively. Here  $r_{ij}$  is the distance between atom i and atom j. The initial condition of the friction simulation was modified to investigate the effect of the temperature, sliding speed, crystal orientation, particle size, and degree of intersection on friction.

## 2.2. Tensile Simulation

Tensile testing is the most commonly used experimental method for determining the elastic modulus. The atomic-level tensile simulation in this investigation is analogous to

FIGURE 2 Schematic of bulk shape SiC model



laboratory tensile tests. In the simulation, the bulk shape 3C-SiC was created because a regular shape more easily examines the relationship between stress and strain. Figure 2 shows the bulk SiC model.

In this model, the atom layers at the bottom of the bulk model along the y-axis were fixed, and a constant velocity was exerted on the top several layers so the model was stretched with a constant strain rate until fracture or failure occurred. These two top and bottom portions were assigned to the "boundary" part, and the rest of the potion was assigned to the "middle" part. The simulation was run in a simulation box with boundary condition of ssp (s: non-periodic and shrinkwrapped, p: periodic) in x, y and z direction, respectively. While the tensile force direction was parallel to y-axis. First, the entire system was relaxed at 300 K under an NVT ensemble using several steps. Then, an NVT ensemble worked on the "middle" part, while the "boundary" part is under an NVE ensemble. After that, the stress-strain curve was drawn to calculate the final elastic modulus. To calculate elastic modulus, the same Hook's Law in macroscopic experiment was used:

$$\sigma = E\epsilon$$
 (3)

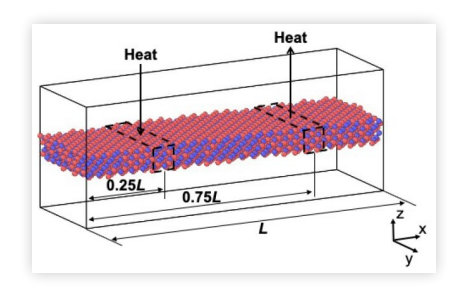
In this equation, E represents elastic modulus,  $\sigma$  is the tensile stress and e is the strain. The strain can also be used to calculate the area of elastic deformation under the stress-strain curve. It should also be noticed that on an atomic scale, there may be some factors that affect the precision of the calculation such as the shape and the size of the model [14]. Therefore, in the future several additional simulations will focus on these influences to obtain a more comprehensive understanding of the elastic modulus at the nano level.

## 2.3. Thermal Conductivity Simulation

LAMMPS provides several ways to evaluate thermal conductivity. Considering that the morphology of the material may affect the final result on a microscopic scale [15], both slab-like shapes and cubic shapes are included. Also, other possible factors influencing thermal conductivity like the temperature and size of the model can be tested. In the case with a slab shape of SiC depicted in Figure 3 below, it was straightforward to add a heat flux into the model.

With PBC applied to all three directions, the SiC thin slab is relaxed to a designated temperature under an NVE ensemble. After the whole system was in a stable status, two thermostats were set up, one with energy added to become a hot region, and the other with energy subtracted to become a cold region. The amount of energy added was equal to that

FIGURE 3 Schematic of a SiC thin slab model with heat flux added



of the energy subtracted. Which resulted in a heat flux in between. Here, the basic idea is related to Fourier's law, which is given by:

$$J = -\kappa \nabla T \tag{4}$$

Where, J is the local heat flux density,  $\kappa$  is the thermal conductivity, and  $\nabla T$  is the temperature gradient along the latitudinal direction of SiC slab. The temperature gradient was created by the heat flux mentioned above, where the same amount of heat was added and subtracted at each time step at the positions of 0.25L and 0.75L, respectively. Based on the slope of the temperature gradient profile, the thermal conductivity was derived.

In this work, the heat flux is defined as:

$$J = \frac{\Delta E}{2A\Delta t} \tag{5}$$

where  $\Delta E$  is the amount of heat added to or subtracted from the slab every  $\Delta t$  timestep, and A is the cross sectional area of the slab. With the value of heat flux determined, the thermal conductivity can be calculated using Equation (4).

When it comes to a cubic model, it's not appropriate to directly set up a hot region and cold region to continuously create energy flow in between due to the morphology of the model. Thus, a different method called equilibrium Green-Kubo formalism was used in this scenario [16, 17]. The Green-Kubo formulas corresponding to the ensemble average of the autocorrelation for the thermal conductivity with respect to the heat flux can be written as:

$$\kappa = \frac{V}{3k_{\rm B}T^2} \int_0^\infty \langle J(0) \cdot J(t) \rangle$$
 (6)

In the formula, V is the volume of the model,  $k_B$  is the Boltzmann constant, which is defined as  $1.380649 \times 10^{-23}$  J·K<sup>-1</sup>, T is the temperature of the system, and J is the heat flux of two-body interactions. In the scenario of two-body interactions, the heat flux is expressed as:

$$J = \frac{1}{V} \left[ \sum_{i} e_{i} \mathbf{v}_{i} - \sum_{i} S_{i} \mathbf{v}_{i} \right] = \frac{1}{V} \left[ \sum_{i} e_{i} \mathbf{v}_{i} - \sum_{i < j} (\mathbf{F}_{ij} \cdot \mathbf{v}_{j}) \mathbf{r}_{ij} \right]$$

$$= \frac{1}{V} \left[ \sum_{i} e_{i} \mathbf{v}_{i} - \frac{1}{2} \sum_{i < j} (\mathbf{F}_{ij} \cdot (\mathbf{v}_{i} + \mathbf{v}_{j})) \mathbf{r}_{ij} \right]$$
(7)

In the first term,  $e_i$  stands for the per-atom energy (kinetic energy and potential energy). In the second term,  $S_i$  is the per-atom stress tensor. The stress tensor multiplies  $v_i$  (velocity of the i-th atom) as a  $3 \times 3$  matrix-vector multiply to yield a vector.  $F_{ij}$  indicates the force on atom i due to atom j and  $r_{ij}$  is the distance between atom i and atom j.

## 3. Results and Discussions

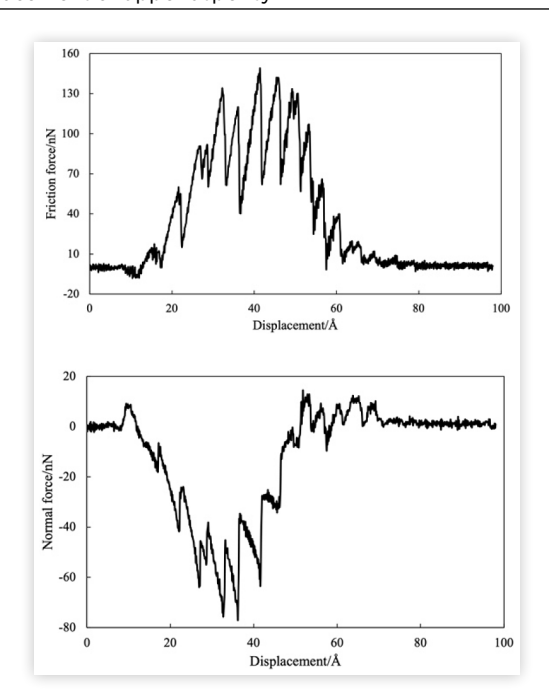
## 3.1. Asperity-Asperity Shear

The whole process of asperity-asperity shear, which is shown in <u>Figure 4</u>, is visualized through Ovito.

In Figure 4, the horizontal axis represents the displacement of the upper asperity during the course of the simulation. For the two profiles, a friction force with a positive value indicates a force is detected on the lower asperity and is directed toward the upper asperity. Similarly, a normal force with a negative value indicates the two asperities are repulsing each other, while a positive value indicates attraction. It can be observed in Figure 4 that the positions where two asperities first make contact, attractive interaction is dominated via the normal force. Both friction force and normal force were averaged for subsequent analysis in order to derive the effective friction coefficient in each friction simulation and facilitate the comparison with the existing data from the literature.

**3.1.1. Effect of Temperature on Friction** The temperature of a brake system is a very important factor which can largely influence overall friction performance. A common range for the temperature of a brake system in an ordinary vehicle is about 300 K to 900 K. Using this temperature range,

**FIGURE 4** Profiles of friction force and normal force versus displacement of upper asperity

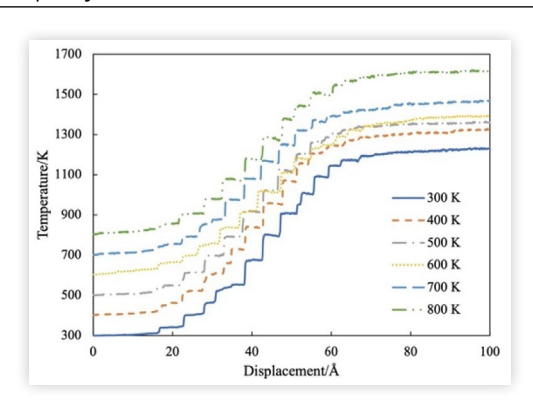


the two SiC asperities, each with a radius of 30 Å and normalized interference of 0.2, were used with initial system temperatures of 300 K, 400 K, 500 K, 600 K, 700 K, and 800 K. The temperature variance with respect to displacement is displayed in Figure 5 (Heat transfer through the air is not taken into consideration).

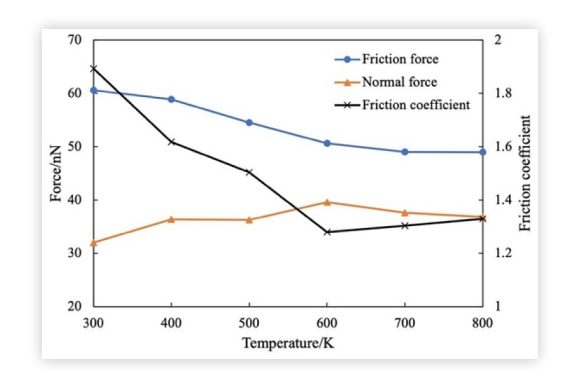
During the friction process, the temperature rises to a certain level as the result of the heat generated. It is intuitive then that with a higher initial temperature, the final temperatures of the asperities will also be higher. The friction and normal forces and the corresponding friction coefficient for each initial temperature are shown below in Figure 6.

Figure 6 indicates the trend of averaged friction force, averaged normal force, and effective friction coefficient for each scenario in Figure 5. It shows that with higher initial temperature, friction force has a downward trend while normal force fluctuates between 32 nN and 40 nN. This also leads to a decrease in friction coefficient with higher initial temperature. In fact, the atoms of SiC will have large vibrations under such high temperatures and this vibration can reduce their resistance to movement. This could help to make the asperities slide with a smaller force when atoms interact with each other. The coefficients of friction are all greater than 1, which may seem alarming. These values are greater than unity, because on a nanoscale adhesive interaction is an important contribution to the friction force between atoms [18]. Adhesive interaction increases the magnitude of the friction coefficient because the friction force becomes larger.

**FIGURE 5** Temperature versus displacement of the upper asperity



**FIGURE 6** Friction force, normal force, and corresponding friction coefficient with initial temperature



**3.1.2. Effect of Sliding Speed on Friction** Considering the driving speed of a vehicle under normal condition, the sliding speed between the brake pad and the disc was given as 10 m/s to 60 m/s with a 10 m/s increment to simulate the asperity friction process using the same interference, asperity radius, and initial temperatures as the previous section. The data derived from the simulation using a temperature of 300 K is exhibited in Figure 7.

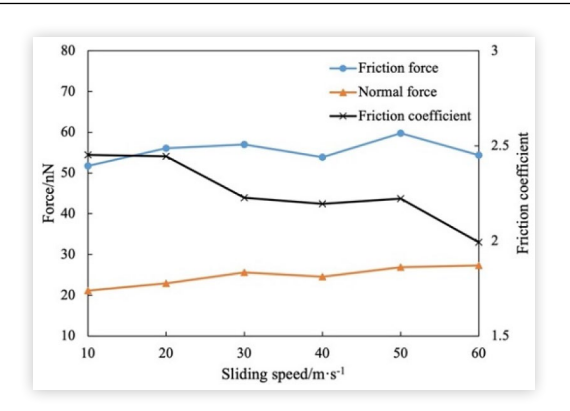
From the result, it seems both friction force and normal force do not exhibit any apparent trend with the change in sliding speed. The calculated effective friction coefficient only changes a small amount (2-2.5). This result indicates that the sliding speed at this scale doesn't have a significant influence on friction performance. Of course, there could be scenarios when the driving speed is lower than 10 m/s, which may show a different influence on friction behavior. Thus, it's our intention to extend our research to lower sliding speeds in the future to get a more comprehensive understanding.

#### 3.1.3. Effect of Degree of Intersection on Friction

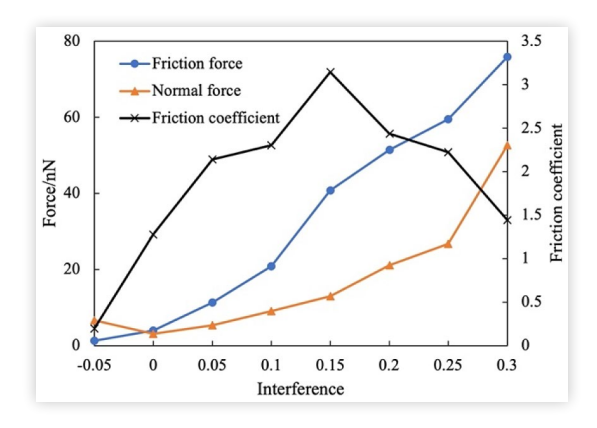
With two asperities sliding relative to each other, the length of overlap in between could be a variable that affects the interaction among atoms, thus, affecting the friction process. To evaluate this parameter, the interference between the asperities was divided by the radius of one asperity to get the normalized interference. Here, the asperity radius is the same as previous sections, which is 30 Å. The sliding speed is 10 m/s with 300 K as the initial temperature of the system.

Figure 8 illustrates how normalized interference affects the forces and the effective friction coefficient. Consider that on a nanoscale, there is also an attraction force between atoms. The initial normalized interference was set from -0.05 to 0.3 with the interval of 0.05; with negative values meaning there is a gap vertically between the two asperities. It is clear to see that both friction force and normal force increase with interference. Typically, the friction force would increase with more interference, since the number of atoms contacting each other would increase and cause larger adhesive forces between the two asperities. However, the normal force also exhibits an increasing trend as interference goes up. By analyzing the change of the normal force with each timestep, this anomaly can be explained by the higher repulsion between two

**FIGURE 7** Friction force, normal force, and corresponding friction coefficient versus sliding speed



**FIGURE 8** Friction force, normal force, and corresponding friction coefficient with normalized interference



asperities caused by larger interference. Further, based on the growth rates of the two forces, the calculated friction coefficient first rises then falls, which shows that the friction force grew faster than the normal force and later the situation was reversed.

**3.1.4. Effect of Particle Size on Friction** Particle size can influence friction as well, because with larger radius asperities, there would be an increase in atoms interacting with each other during the friction process leading to a larger friction force. It is clearly shown in Figure 9.

The asperity radius for each simulation is 20, 30, 40, 50, and 60 Å, with a sliding speed of 10 m/s, initial temperature of 300K, and an interference of 0.2. The results show that both friction force and normal force get larger with increased asperity size. It's evident that interaction between larger asperities cause more contact among atoms, leading to higher acting forces. The friction coefficient is thereby reduced because of the faster increase of normal force than friction force.

#### 3.1.5. Effect of Lattice Orientation on Friction

In order to evaluate the effect that lattice orientation has on friction coefficient for the asperities, different angles of lattice were tested. The result is shown in <u>Figure 10</u>.

The lattice orientations of 0-45° with an increment of 5° were used. Different from the work done by Vadgama et al.

**FIGURE 9** Friction force, normal force, and corresponding friction coefficient versus asperity radius

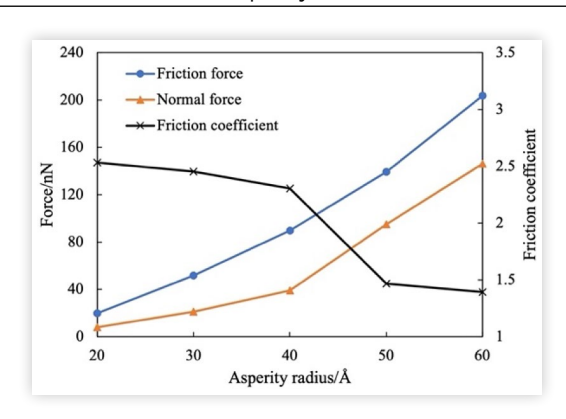
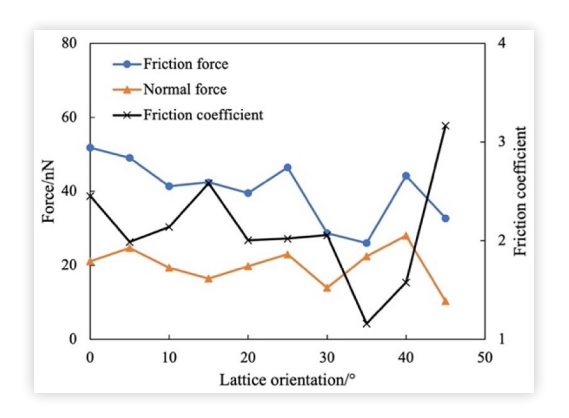


**FIGURE 10** Friction force, normal force, and corresponding friction coefficient versus lattice orientation



[10], there is no clear relationship between forces and lattice orientation for SiC. However, when it comes to 45°, the interaction is weaker than other orientations, which is similar to that with lattice orientation of 0, but with a relatively small number (maximal value 50 nN for 0 and 20 nN for 45°). It also turns out that the frictional wear is enhanced significantly between 5° and 40°, compared to 0 and 45°. Based on this analysis and the visualization of friction, the reason for large friction wear, and the conversion from repulsive force to attractive force, comes from higher deformation and material transfer due to the lattice orientation being not close to the sliding plane (111), which is more prone to slip [19, 20]. A comparison between a 45° orientation and 25° orientation can be seen in Figure 11.

When the lattice orientation is 45°, the deformation or material transfer of the asperities is much lower than the case of 25°. This results in lower wear and forces because the 45° orientation is more parallel to the (111) plane.

Table 1 compares the results with similar works, where cases 2-4 are from literature [10, 21, 22] and case 1 is the results of this investigation. Although there is no direct data that can be used to examine the validity of the result of the friction simulation in this work, it is not surprising to see that the simulation results are reasonable, since the MD simulation results from different works are close to each other and consistently greater than the experimental results.

**FIGURE 11** Deformation after friction for 25° and 45° lattice orientations

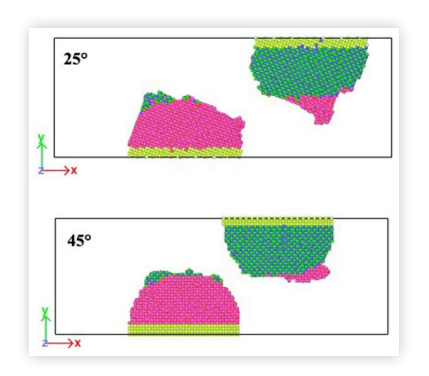


**TABLE 1** Friction coefficient from different works

Results from different works				
Case	1	2	3	4
Material	SiC	SiC	Cu	Cu
shape	Asperity	Ring	Asperity	Block
Туре	MD	Experiment	MD	MD
Temperature	300 K	Ambient	300 K	293 K
Load	21.1 nN	6.6 N	13.5 nN	150.0 nN
Sliding speed (m/s)	10	0.897	10	100
Friction coefficient	2.45	0.2	2.25	2.2

### 3.2. Elastic Modulus of SiC

During the tensile test simulations, there was no significant change in the appearance of the block at first, then it became obvious, with the formation of necking or fracture, that deformation was occurring somewhere along the length of the sample. To evaluate size effects on the elastic modulus of SiC block at the atomic level, two types of modifications were applied to change the size of the model. First was to change the length of the block only in the x direction, the second was to change its length in both x and y directions. It is apparent that the change in length both in a single direction and two directions show very similar effects on the slope of the stressstrain curve during elastic deformation. The elastic modulus increases from 270.95 GPa to 290.81 GPa and 313.61 GPa as the original length of the model in x direction increases from 20 Å to 40 Å and 60 Å. When both lengths in x- and y- directions increase with the same magnitude, the curves for each case exhibit the same tendency of growth in slope, which is 270.95 GPa, 292.76 GPa, and 310.82 GPa, before the transformation from elastic deformation to plastic deformation. A larger model could have a higher elastic modulus with similar shapes. Figure 12 exhibits the stress-stain curves of SiC blocks with different lengths along x- direction.

<u>Table 2</u> below lists the results derived from the simulation (Case 1) and other works (Case 2-5) [13, 23].

The comparison shows that the elastic modulus obtained from large model size in this paper is similar to but not the same as other results found in literature. Based on this

**FIGURE 12** Stress-strain curves for SiC blocks of different sizes

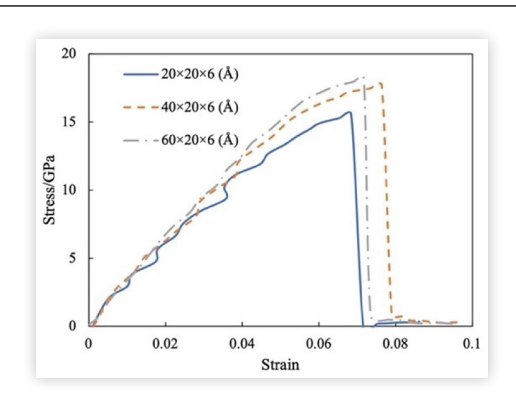


**TABLE 2** Elastic modulus reported in literature

Case	Material	Туре	Elastic Modulus (GPa)
1	β-SiC	MD	270.95-313.61
2	β-SiC	MD	313.6
3	$\alpha\text{-SiC}$	MD	323.4
4	β-SiC	Experiment	314.2
5	β-SiC	Experiment	392-448

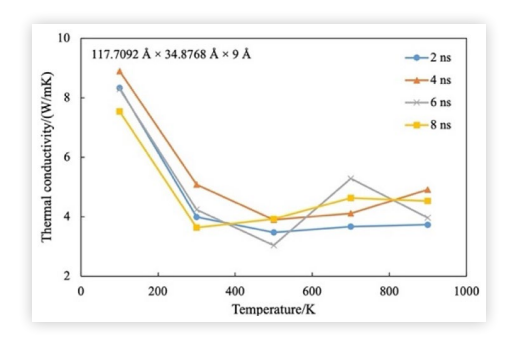
discovery, the size effect could be overcome with large dimensions and elastic modulus is expected to get close to real value. This method of testing mechanical properties such as elastic modulus may help study their relationship to tribological properties and provide new ideas for improving tribological properties.

## 3.3. Thermal Conductivity of SiC

SiC slabs with dimensions of 117.709 Å  $\times$  34.877 Å  $\times$  9 Å, 239.778 Å  $\times$  34.877 Å  $\times$  9 Å, and 357.487 Å  $\times$  34.877 Å  $\times$  9 Å were employed in this simulation. The cross-sectional area was known for each case.  $80 \times 0.00431$  eV ( $\Delta E$ ) was added and subtracted from the slab every 1000 timesteps ( $\Delta t$ ). The system was first constructed and relaxed at 100 K. Then, the heat flux was introduced to the system. The heat flux simulation in the thin slab SiC gives the temperature distribution along the slab. Then based on the slope of the temperature variance between hot and cold regions, the thermal conductivity could be derived. The system was heated from 100 K to 900 K with steps of 200 K. It should be noted that although the trend of thermal conductivity for different relaxation times could be similar, the heat flux at the beginning of the relaxation may not have been stable yet. This would result in inaccurate calculations of thermal conductivity. An 8 ns relaxation was applied to each stage so that the heat flux would remain stable. The value of thermal conductivity of the SiC slab along the x direction versus temperature is shown in Figure 13.

It turns out that, from the beginning of the simulation when the heat flux just formed, to the time of 8 ns when the heat flux had reached a stable state approximately, the measured thermal conductivity didn't change much, aside from dropping very fast from a relatively high value to a low level as the temperature increasing from 100 K to 300 K. Then

**FIGURE 13** Thermal conductivity of SiC slab along x direction versus temperature at different relaxation times



it remained stable while the temperature kept increasing to 900 K. The results from different sized slabs do not show a very obvious difference either. According to literature [15], there could be an influence of finite size effects regarding the phonon mean free path. Literature states when the length of heat flux is shorter than the maximum phonon mean free path, the material always behaves as if it had higher thermal conductivity with a longer mean free path of phonons. This effect would disappear once the heat flux length exceeds the maximum phonon mean free path. Based on this theory, it is likely the sizes of the models in all three cases are here beyond the maximum phonon mean free path such that no significant difference is observed on thermal conductivity values.

The relationship between thermal conductivity and temperature are shown in <u>Figure 13</u> and can be explained by the phonon kinetic theory [24]. The theory gives the formula as

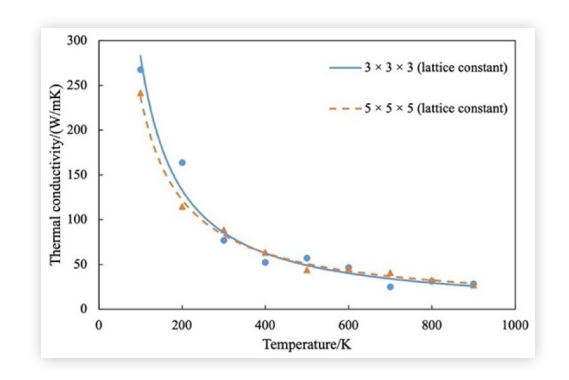
$$\kappa = \frac{1}{3} C_{\rm v} \nu_{\rm p} \lambda \tag{8}$$

where  $C_{\rm v}$  is the specific heat at constant volume,  $\nu_{\rm p}$  is the average phonon velocity, and  $\lambda$  is the phonon mean free path. Usually,  $\nu_{\rm p}$  is a constant and  $\lambda$  decreases as temperature goes up. [25] When the temperature is very low,  $C_{\rm v}$  is proportional to the cubic temperature. When the temperature increases,  $C_{\rm v}$  approaches a constant while  $\lambda$  continues to decrease. That's why thermal conductivity has a huge drop of thermal conductivity in the low-temperature region, and a decreasing trend when the temperature rises.

Cubic SiC, another common type, was considered in the work of thermal conductivity evaluation. The sizes of  $3 \times 3 \times 3$  and  $5 \times 5 \times 5$  (lattice constant) were implemented with a Green-Kubo equilibrium MD method to calculate thermal conductivity from 100 K to 900 K with a step size of 100 K. Figure 14 shows the result after curve fitting.

There is a huge difference in magnitude of thermal conductivity between cubic SiC and SiC thin slab with the same material and potential. This indicates that the magnitude of thermal conductivity for SiC is related to the shape of the material. The thermal conductivity of cubic SiC decreases from about 267.64 W/mK at 100 K to about 28.33 W/mK at 900 K for the small model. For the larger model, in the low-temperature range, there is an obvious difference in magnitude, but in the high-temperature range the results from the two models are approximately equivalent. One can also interpolate the value of thermal conductivity for this specific model

**FIGURE 14** Thermal conductivity of cubic SiC at various temperatures



at different temperatures after curve fitting. This trend is similar to the results reported by other works, however the magnitude is slightly different. This could be due to different potentials and sizes of the models used [26, 27]. In general, the understanding of thermal properties may give new insights into the research of TMI and the best method for mitigation.

## 4. Conclusions

In this paper, an MD study of the evaluation of 3C-SiC friction, tensile test, and the calculation of thermal conductivity was preformed using LAMMPS. Corresponding properties were analyzed and discussed. The results were investigated by comparing with the existing data. The designed model for each scenario was validated to help understand the mechanism of friction on a nanoscale and the effects of mechanical and thermal properties on friction. The conclusions of the investigation are as follows:

- For SiC friction on a nanoscale, as asperities come into contact and slide to relative each other, there is not only friction force between them, but also an adhesive force due to the attractive interaction between the atoms.
- Based on the initial conditions set in this work, the profile of friction force, normal force, and corresponding friction coefficient can be derived and analyzed. Also, the computed friction coefficient showed agreement with existing data found in literature.
- 3. The tensile test of SiC on a nanoscale indicates that the dimension of the material has an influence on elastic deformation. An increase in the size of the model leads to a larger Young's modulus due to the size effect.
- 4. Different shapes of the model will create different thermal conductivities for SiC. A SiC thin slab has a much lower thermal conductivity compared to a cubic SiC. The thermal conductivity decreases with temperature for both types of shapes. The drop rate is much higher at a low-temperature range than at a high-temperature range, and the value of thermal conductivity remains stable at high temperatures.

## Acknowledgment

Support for this work, provided by the National Science Foundation under Contract (No. 1928876), is gratefully acknowledged.

## References

1. Lu, Y., "A Combinatorial Approach for Automotive Friction Materials: Effects of Ingredients on Friction Performance," *Composites science and technology* 66, no. 3 (2006): 591-598, doi:10.1016/j.compscitech.2005.05.032.

- Sriwiboon, M., Tiempan, N., Kaewlob, K., and Rhee, S., "Non-Asbestos Organic (NAO) Disc Pad Wear Behavior: Divergence of Thickness Loss and Weight Loss," SAE Technical Paper 2018-01-1866 (2018). https://doi. org/10.4271/2018-01-1866.
- Solomon, D.G. and Berhan, M.N., "Characterization of Friction Material Formulations for Brake Pads," in: , Proceedings of the World Congress on Engineering 2007 Vol II WCE 2007, July 2 - 4, (London, U.K., 2007), 2007.
- Sanguineti, A., Samela, A., Rampinelli, F., Bottalico, L. et al., "Cementitious-Based Brake Pads Technology: Performance, Low Energy Consumption, Emission Drop," SAE Technical Paper 2018-01-1867 (2018). https://doi.org/10.4271/2018-01-1867
- Aquatic Life Ambient Water Quality Criteria: Copper, "2007 Rev. United States Environmental Protection Agency, Office of Water," in: , Office of Science and Technology, (2007).
- Yi, Y.-B., "Perturbation Methods in Thermoelastic Instability (TEI) with Finite Element Implementation," in: , *Encyclopedia of Thermal Stresses*, (Springer Netherlands), 3635-3641, doi:10.1007/978-94-007-2739-7\_154.
- Zhao, J., Ma, B., and Li, H., "Investigation of Thermoelastic Instabilities of Wet Clutches," in: , 2013 IEEE International Symposium on Assembly and Manufacturing (ISAM), IEEE, (2013), 69-72, doi:10.1109/ISAM.2013.6643490.
- 8. Plimpton, S., "Fast Parallel Algorithms for Short-Range Molecular Dynamics," *Journal of computational physics* 117, no. 1 (1995): 1-19, doi:10.1006/jcph.1995.1039.
- Stukowski, A., "Visualization and Analysis of Atomistic Simulation Data with OVITO-the Open Visualization Tool," Modelling and simulation in materials science and engineering 18, no. 1 (2010): 015012, doi:10.1088/0965-0393/18/1/015012.
- Vadgama, B.N., Jackson, R.L., and Harris, D.K., "Molecular Scale Analysis of Dry Sliding Copper Asperities," *Applied nanoscience* 5, no. 4 (2015): 469-480, doi:10.1007/s13204-014-0339-9.
- 11. Zhong, J., Adams, J.B., and Hector, L.G., "Molecular Dynamics Simulations of Asperity Shear in Aluminum," *Journal of applied physics* 94, no. 7 (2003): 4306-4314, doi:10.1063/1.1558966.
- 12. Sharma, S., Molecular Dynamics Simulation of Nanocomposites Using BIOVIA Materials Studio (Lammps and Gromacs: Elsevier, 2019)
- Vashishta, K., "Interaction Potential for Silicon Carbide: A
   Molecular Dynamics Study of Elastic Constants and
   Vibrational Density of States for Crystalline and Amorphous
   Silicon Carbide," *Journal of applied physics* 101, no. 10 (2007):
   103515, doi:10.1063/1.2724570.
- 14. Safont Camprubí, G., *Mechanical Properties at Nano-level*, Published online 2010.
- Papanikolaou, N., "Lattice Thermal Conductivity of SiC Nanowires," *Journal of physics Condensed matter* 20, no. 13 (2008): 135201, doi:10.1088/0953-8984/20/13/135201.
- Green, M.S., "Markoff Random Processes and the Statistical Mechanics of Time-dependent Phenomena. II. Irreversible Processes in Fluids," *The Journal of chemical physics* 22, no. 3 (1954): 398-413, doi:10.1063/1.1740082.

- Kubo, R., "Statistical-Mechanical Theory of Irreversible Processes. I. General Theory and Simple Applications to Magnetic and Conduction Problems," *Journal of the physical* society of Japan 12, no. 6 (1957): 570-586, doi:10.1143/ jpsj.12.570.
- 18. Hu, X. and Martini, A., "Atomistic Simulation of the Effect of Roughness on Nanoscale Wear," *Computational materials science* 102 (2015): 208-212, doi:10.1016/j. commatsci.2015.02.036.
- 19. Chen, H.-P., Kalia, R.K., Nakano, A., Vashishta, P. et al., "Multimillion-atom Nanoindentation Simulation of Crystalline Silicon Carbide: Orientation Dependence and Anisotropic Pileup," *Journal of applied physics* 102, no. 6 (2007): 063514-063514-9, doi:10.1063/1.2781324.
- 20. Zhao, L., Zhang, J., Pfetzing, J., Alam, M. et al., "Depth-sensing Ductile and Brittle Deformation in 3C-SiC under Berkovich Nanoindentation," *Materials & Design* 197 (2021): 109223, doi:10.1016/j.matdes.2020.109223.
- 21. Zhang, W., Yamashita, S., and Kita, H., "Progress in Tribological Research of SiC Ceramics in Unlubricated Sliding-A Review," *Materials & design* 190 (2020): 108528, doi:10.1016/j.matdes.2020.108528.
- 22. Chien, C.-H., Wang, C.-T., Tsai, C.-H., Yang, P.-F. et al., "Temperature Effect on Kinetic Friction Characteristics of Cu Substrate Composed by Single Crystal and Polycrystalline Structures," *Computational materials science* 117 (2016): 412-421, doi:10.1016/j.commatsci.2016.01.043.
- 23. Harris, G.L., Properties of Silicon Carbide, 1995.
- 24. Liu, Q., Luo, H., Wang, L., and Shen, S., "Tuning the Thermal Conductivity of Silicon Carbide by Twin Boundary: A Molecular Dynamics Study," *Journal of physics D, Applied*

- *physics* 50, no. 6 (2017): 65108, doi:<u>10.1088/1361-6463/aa553d</u>.
- Tritt, T.M., Thermal Conductivity: Theory, Properties, and Applications (Kluwer Academic/Plenum Publishers, 2004)
- Szpunar, M., "Atomistic Modeling of Thermo-mechanical Properties of Cubic SiC," *Journal of the American Ceramic* Society 101, no. 10 (2018): 4753-4762, doi:10.1111/jace.15712.
- Li, J., Porter, L., and Yip, S., "Atomistic Modeling of Finite-temperature Properties of Crystalline β-SiC: II. Thermal Conductivity and Effects of Point Defects," *Journal of nuclear materials* 255, no. 2 (1998): 139-152, doi:10.1016/S0022-3115(98)00034-8.

### **Contact Information**

#### Yizhan Zhang

PhD student
Mechanical & Materials Engineering
University of Denver
2155 E Wesley Ave
Denver, CO 80208
Yizhan.Zhang@du.edu

#### Yun-Bo Yi, Ph.D.

Professor

Mechanical & Materials Engineering University of Denver 2155 E Wesley Ave Denver, CO 80208 Yun-Bo.Yi@du.edu

Phone: 303-871-2228

<sup>© 2021</sup> SAE International. All rights reserved. No part of this publication may be reproduced, stored in a retrieval system, or transmitted, in any form or by any means, electronic, mechanical, photocopying, recording, or otherwise, without the prior written permission of SAE International.